Available online at www.sciencedirect.com
SCIENCE DIRECT®
Journal of Computational Physics 213 (2006) 184–204
JOURNAL OF COMPUTATIONAL PHYSICS
www.elsevier.com/locate/jcp

Analysis of stability and accuracy of finite-difference schemes on a skewed mesh

Donghyun You [a,*], Rajat Mittal [b], Meng Wang [a], Parviz Moin [a]

[a] Center for Turbulence Research, Stanford University, Stanford, CA 94305, United States
[b] Department of Mechanical and Aerospace Engineering, George Washington University, Washington, DC 20052, United States

Received 19 April 2005; received in revised form 7 August 2005; accepted 8 August 2005
Available online 15 September 2005

Abstract

Numerical stability and accuracy of finite-difference schemes on a skewed non-uniform mesh are investigated to provide guidelines for mesh design and for devising appropriate solution methods when mesh skewness is unavoidable. In the current analysis, a linear advection–diffusion equation in a Cartesian coordinate system is transformed into a curvilinear one corresponding to a skewed mesh. A finite-difference approximation of the transformed equation leads to the leading-order error terms which are responsible for time-step restrictions and numerical instability. A truncation error analysis of central-difference approximation reveals the effects of mesh non-uniformity and skewness on the solution quality. In addition, a modified wavenumber analysis is performed for the central- and upwind-difference schemes coupled with time-integration methods, to examine the effects of mesh skewness angle and flow direction relative to the mesh angle on the numerical stability. In general, severe mesh skewness leads to restrictions on the allowable cell Peclet number and time-step size and also increases phase and amplitude errors.

Keywords: Mesh skewness; Numerical stability; Numerical accuracy; Finite-difference scheme; Advection–diffusion equation

0. Introduction

Finite-difference schemes have been used widely to obtain numerical solutions of governing equations for fluid flow inside or around complex geometries. Geometric complexity and complicated boundary conditions often necessitate the use of skewed meshes, which can have a strong effect on the numerical stability properties and accuracy of the scheme. The detrimental effects of highly skewed meshes on the

* Corresponding author. Tel.: +1 650 723 9596; fax: +1 650 723 9617.
E-mail address: dyou@stanford.edu (D. You).

0021-9991/$ - see front matter © 2005 Elsevier Inc. All rights reserved.
doi:10.1016/j.jcp.2005.08.007

solution quality and numerical stability have been reported in a number of recent large-eddy simulations [1–3]. For example, You et al. [1] observed severe numerical instability in a large-eddy simulations of rotor tip-leakage flow which advects through a highly skewed mesh. By performing numerical tests, they found that a simulation employing the divergence or skew-symmetric form of the nonlinear terms in the Navier–Stokes equations produces a more stable solution than employing the advection form. Mittal et al. [2] and Wang and Moin [3] also observed numerical instability associated with mesh skewness in large eddy simulations of flow over a turbine blade and a naval hydrofoil, respectively. The motivation of the present study is to gain a better understanding of the mesh skewness related instability in large-eddy simulations with non-dissipative numerical schemes and to devise appropriate remedies when severe mesh skewness is unavoidable.

As an example, Fig. 1 shows two meshes designed for flow over a compressor blade with a large stagger angle of 57°. The mesh in Fig. 1(a) is skewed everywhere, whereas in Fig. 1(b), mesh skewness is limited to the blade chord region, and the inlet and outlet sections are Cartesian. Except for the skewness angle, the

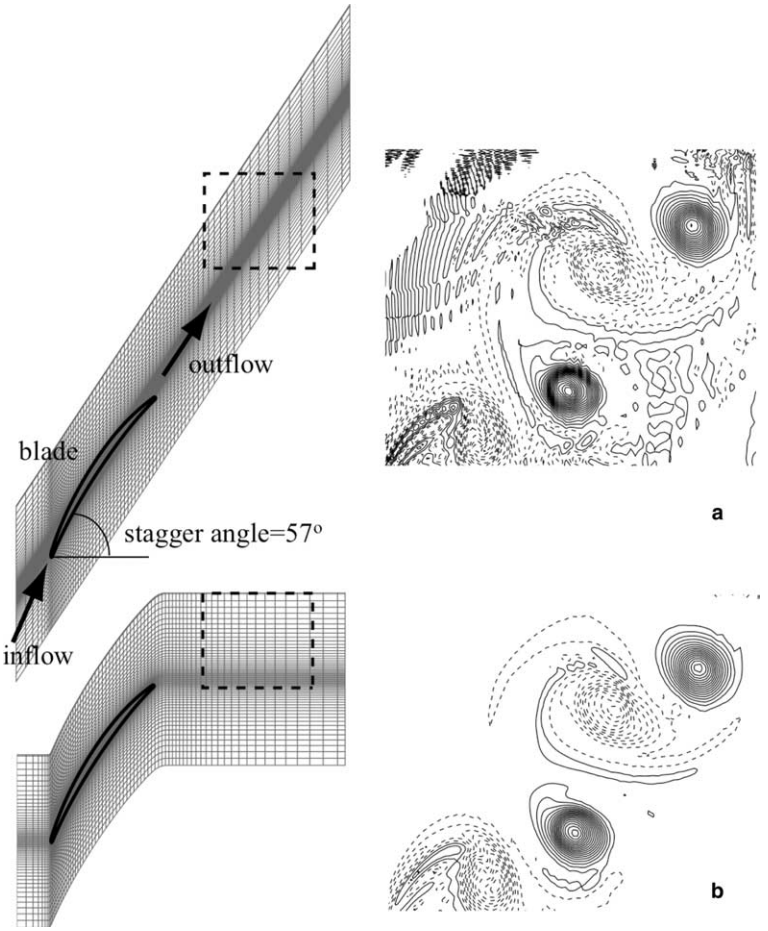

Fig. 1. Two computational meshes used in conjunction with immersed boundary method for flow over a two-dimensional compressor blade (1/6 lines plotted) and contours of instantaneous spanwise vorticity in the wake. Mesh size of $449 \times 351 \times 129$, same grid spacing, and Reynolds number of 10^4 based on the blade chord and inflow free-stream velocity are employed for both (a) and (b). 40 contour levels in the range of -20 to 20 are shown. Negative values are dashed.

same mesh parameters such as spacings and stretching ratios are employed for both meshes. Since the grid lines are better aligned with the flow direction in the first case, better resolution is expected in the wake. However, the second grid, which is essentially Cartesian in the wake, exhibits better numerical stability characteristics. It is found that numerical instability becomes a serious problem in the blade wake when the vortex is convected along the skewed mesh.

In this example, it is also noted that numerical instability is related to not only the numerical scheme and mesh skewness but also the flow features simulated and mesh resolution. Numerical instability represented by the 'wiggles' is less severe or non-existent in the blade boundary layer region, where the mesh is also highly skewed as shown in Fig. 1. A major difference between the skewed mesh regions around the blade and in the downstream wake is the flow characteristics and mesh resolution. In contrast to the strong vortex structures in the wake, the flow near the blade surfaces is dominated by a parallel boundary layer flow aligned to the one set of grid lines with better resolution. In Reynolds-averaged Navier–Stokes (RANS) computations of related problems (e.g. [4–6]), numerical wiggles are generally absent because of strong dissipation, and hence the mesh skewness effects are ignored, even though they can affect the accuracy of the solution.

Truncation error analysis has been a popular tool to study the effects of mesh non-orthogonality and skewness. Thompson et al. [7] showed that the truncation errors from a finite-difference approximation of the first derivative of a function on a non-orthogonal mesh are significantly amplified if the mesh becomes highly skewed. The truncation error analysis of Lee and Tsuei [8], based on the upwind discretization for the advection terms in a curvilinear coordinate system, revealed that the errors are affected by the grid cell size and skewness angle, as well as the flow direction. Recently, Sankaranarayanan and Spaulding [9] investigated the effects of grid non-orthogonality on the solution of the shallow water equations, which only include the first-order temporal- and spatial-derivative terms. They concluded that truncation errors, essentially the dispersion errors, of the finite-difference approximations increase with grid skewness. Mesh skewness has also been identified as the source of the numerical dispersion error and reduced numerical stability in the time-marching equation for an electric field in electro-magnetic applications [10,11].

However, the effects of mesh skewness on the quality of the numerical solution and on the procedure to obtain the solution of full Navier–Stokes or even linear advection–diffusion equations are still not well understood. The truncation error analysis based on spatial discretization alone, as in [7,8], cannot elucidate the detailed effects of mesh skewness on the stability of numerical integration. Also, as will be shown later, mesh skewness significantly influences the numerical errors associated with the discretization of diffusion terms and thereby results in stability problems for the advection–diffusion type equations. As the large-eddy simulation technique, which is relatively sensitive to mesh quality, is applied to increasingly more complex geometries, an improved understanding of the effects of mesh skewness and non-uniformity on the solution and the numerical procedure is of great importance.

The objective of this study is to examine the cause of numerical instability in finite-difference approximations of partial differential equations on a skewed mesh, and its effect on the solution quality. For this purpose, a finite-difference representation of an advection–diffusion equation involving temporal and spatial derivatives on a skewed mesh is constructed by a coordinate transformation. The derivatives with respect to the curvilinear coordinates are then replaced with finite-difference expressions on a uniform grid in the transformed domain. Unlike previous investigations, the present study takes a more comprehensive approach in that the unsteady advection–diffusion equation is analyzed as a whole, and various spatial-discretization schemes and time-integration schemes are considered. Both the truncation error and modified wave number analyses are performed to reveal the various effects of the mesh skewness and non-uniformity.

Specific goals of the present study are (i) to gain a physical insight into the characteristics of spatial discretization errors related to the mesh non-uniformity and skewness and (ii) to understand the effect of mesh

skewness on the solution procedure including both the spatial discretization and temporal integration. To achieve these goals, the modified equation for a semi-discretized system will first be derived to reveal the leading order truncation error terms causing numerical instability. Then, a modified wavenumber analysis will be utilized to investigate the effects of mesh-skewness on the solution procedure including the characteristics of numerical errors and the maximum allowable time-step size for the temporally and spatially discretized equation in the computational domain.

1. Truncation error analysis

The Taylor's series expansion of any function $f(\xi)$ describing a non-uniform mesh distribution along $\xi = \frac{j}{N}$ results in:

$$f(\xi) = \begin{cases} f'(0)\xi + \frac{f''(0)}{2!}\xi^2 + \frac{f'''(0)}{3!}\xi^3 + \cdots, \\ f'(0)\left(\frac{j}{N}\right) + \frac{f''(0)}{2!}\left(\frac{j}{N}\right)^2 + \frac{f'''(0)}{3!}\left(\frac{j}{N}\right)^3 + \cdots, \end{cases} \tag{1}$$

where $j = 0, 1, 2, \ldots, N$, and N is the number of mesh points. $f(0)$ has been set to zero. For example, the exponential and hyperbolic tangent functions commonly used for non-uniform mesh generations are given by:

$$f(\xi) = \frac{1}{\exp(\beta) - 1}\{\exp(\beta\xi) - 1\}, \tag{2}$$

and

$$f(\xi) = 1 - \frac{\tanh[\beta(1-\xi)]}{\tanh(\beta)}. \tag{3}$$

These can all be expressed as Eq. (1).

In this study, a stretched or compressed and skewed mesh with a constant skewness angle in a two-dimensional physical domain (x, y), as shown in Fig. 2, is constructed using a mapping function which consists of the first two terms in Eq. (1):

$$(x, y) = (a_0\xi + a_1\xi^2, (a_0\xi + a_1\xi^2)\tan\theta + b_0\eta + b_1\eta^2), \tag{4}$$

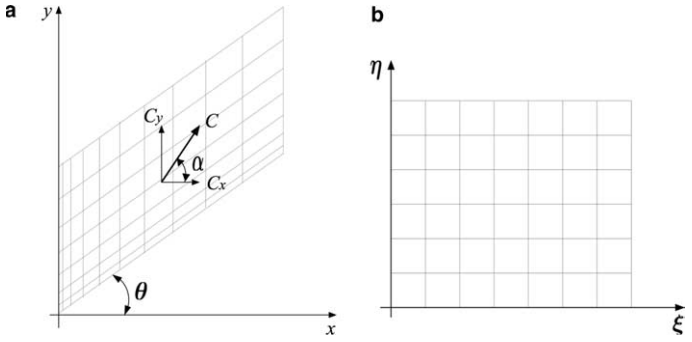

Fig. 2. Coordinate systems and definitions of mesh skewness angle, flow direction, and convection velocity: (a) physical domain; (b) computational domain.

where a_0, a_1, b_0, and b_1 are constants representing mesh spacing and stretching/compression in the x and y directions with ξ and η being independent variables in the transformed generalized coordinates in the computational domain (ξ,η). θ is the mesh-skewness angle as defined in Fig. 2.

The derivatives of independent variables in the Cartesian coordinates with respect to those in the transformed coordinates are:

$$\begin{aligned} &x_\xi = a_0 + 2a_1\xi, \quad x_{\xi\xi} = 2a_1, \quad x_{\xi\xi\xi} = 0,\\ &x_\eta = 0, \quad x_{\eta\eta} = 0, \quad x_{\eta\eta\eta} = 0,\\ &y_\xi = (a_0 + 2a_1\xi)\tan\theta, \quad y_{\xi\xi} = 2a_1\tan\theta, \quad y_{\xi\xi\xi} = 0,\\ &y_\eta = b_0 + 2b_1\eta, \quad y_{\eta\eta} = 2b_1, \quad y_{\eta\eta\eta} = 0. \end{aligned} \tag{5}$$

Chain rules are utilized to relate metric coefficients in both coordinates as:

$$\begin{pmatrix} \xi_x & \eta_x \\ \xi_y & \eta_y \end{pmatrix} = \begin{pmatrix} x_\xi & y_\xi \\ x_\eta & y_\eta \end{pmatrix}^{-1} = \begin{pmatrix} 1/x_\xi & -y_\xi/x_\xi y_\eta \\ 0 & 1/y_\eta \end{pmatrix}, \tag{6}$$

$$\begin{pmatrix} \xi_x & 0 & 0 & \eta_x & 0 \\ \xi_{xx} & \xi_x^2 & 2\xi_x\eta_x & \eta_{xx} & \eta_x^2 \\ 0 & 0 & \xi_x\eta_y & \eta_{xy} & \eta_x\eta_y \\ 0 & 0 & 0 & \eta_y & 0 \\ 0 & 0 & 0 & \eta_{yy} & \eta_y^2 \end{pmatrix} = \begin{pmatrix} x_\xi & 0 & 0 & y_\xi & 0 \\ x_{\xi\xi} & x_\xi^2 & 2x_\xi y_\xi & y_{\xi\xi} & y_\xi^2 \\ 0 & 0 & x_\xi y_\eta & 0 & y_\xi y_\eta \\ 0 & 0 & 0 & y_\eta & 0 \\ 0 & 0 & 0 & y_{\eta\eta} & y_\eta^2 \end{pmatrix}^{-1}. \tag{7}$$

A combination of Eqs. (6) and (7) with Eq. (5) results in:

$$\begin{aligned} &\xi_x = \frac{1}{a_0 + 2a_1\xi}, \quad \xi_y = 0, \quad \xi_{xx} = \frac{-2a_1}{(a_0 + 2a_1\xi)^3},\\ &\eta_x = \frac{-\tan\theta}{b_0 + 2b_1\eta}, \quad \eta_y = \frac{1}{b_0 + 2b_1\eta},\\ &\eta_{xx} = \frac{-2b_1\tan^2\theta}{(b_0 + 2b_1\eta)^3}, \quad \eta_{xy} = \frac{2b_1\tan\theta}{(b_0 + 2b_1\eta)^3}, \quad \eta_{yy} = \frac{-2b_1}{(b_0 + 2b_1\eta)^3}. \end{aligned} \tag{8}$$

To facilitate the analysis, the two-dimensional linear advection–diffusion equation is considered instead of the Navier–Stokes equations:

$$\frac{\partial u}{\partial t} + \tilde{C}^x\frac{\partial u}{\partial x} + \tilde{C}^y\frac{\partial u}{\partial y} = \frac{1}{Re}\left(\frac{\partial^2 u}{\partial x^2} + \frac{\partial^2 u}{\partial y^2}\right). \tag{9}$$

All the coordinate variables, velocity components, and time are non-dimensionalized by the reference length scale L, the convection velocity C, and L/C. $\tilde{C}^x(= C^x/C = \cos\alpha)$ and $\tilde{C}^y(= C^y/C = \sin\alpha)$ are the non-dimensionalized convection velocities in the x and y directions, respectively, and $Re = CL/v$, where v is viscosity. The coordinate transformation of Eq. (9) with respect to ξ and η results in:

$$\frac{\partial u}{\partial t} + (\xi_x u_\xi + \eta_x u_\eta)\cos\alpha + (\eta_y u_\eta)\sin\alpha = \frac{1}{Re}(\xi_{xx}u_\xi + \xi_x^2 u_{\xi\xi} + 2\xi_x\eta_x u_{\xi\eta} + \eta_{xx}u_\eta + \eta_x^2 u_{\eta\eta} + \eta_{yy}u_\eta + \eta_y^2 u_{\eta\eta}). \tag{10}$$

A semi-discretized equation is constructed by treating the spatial derivatives in Eq. (10) with the following second-order central-difference approximations:

$$\begin{aligned}
\frac{\delta u}{\delta \xi} &= u_\xi + \frac{\Delta\xi^2}{6}u_{\xi\xi\xi} + \mathrm{O}(\Delta\xi^4),\\
\frac{\delta^2 u}{\delta \xi^2} &= u_{\xi\xi} + \frac{\Delta\xi^2}{12}u_{\xi\xi\xi\xi} + \mathrm{O}(\Delta\xi^4),\\
\frac{\delta u}{\delta \eta} &= u_\eta + \frac{\Delta\eta^2}{6}u_{\eta\eta\eta} + \mathrm{O}(\Delta\eta^4),\\
\frac{\delta^2 u}{\delta \eta^2} &= u_{\eta\eta} + \frac{\Delta\eta^2}{12}u_{\eta\eta\eta\eta} + \mathrm{O}(\Delta\eta^4),\\
\frac{\delta^2 u}{\delta\xi\,\delta\eta} &= \frac{\delta^2 u}{\delta\eta\,\delta\xi} = u_{\xi\eta} + \frac{\Delta\xi^2}{6}u_{\xi\xi\xi\eta} + \frac{\Delta\eta^2}{6}u_{\eta\eta\eta\xi} + \mathrm{O}(\Delta\xi^4, \Delta\eta^4).
\end{aligned} \tag{11}$$

Finally, an inverse coordinate transformation of the semi-discretized equation using chain rules, in combination with Eqs. (5) and (8) results in the modified equation in the physical domain:

$$\frac{\partial u}{\partial t} + \frac{\partial u}{\partial x}\cos\alpha + \frac{\partial u}{\partial y}\sin\alpha - \frac{1}{Re}\left(\frac{\partial^2 u}{\partial x^2} + \frac{\partial^2 u}{\partial y^2}\right) = \mathit{Error}. \tag{12}$$

Error on the right-hand side of Eq. (12) is arranged in the following form:

$$\begin{aligned}
\mathit{Error} = {} & A_1u_{xx} + A_2u_{xy} + A_3u_{yy} + B_1u_{xxx} + B_2u_{xxy} + B_3u_{xyy} + B_4u_{yyy} + C_1u_{xxxx} + C_2u_{xxxy} + C_3u_{xxyy}\\
& + C_4u_{xyyy} + C_5u_{yyyy},
\end{aligned} \tag{13}$$

where coefficients A_i, B_i, and C_i are categorized in terms of the source of the errors in Table 1.

The following relations are applied to relate the grid spacings in the computational domain to those in the physical domain:

$$\begin{aligned}
\Delta\xi_{i,j} = \Delta\xi &= (\xi_x\Delta x)_{i,j} + (\xi_y\Delta x)_{i,j} = \frac{\Delta x_i}{a_0 + 2a_1\xi_i} = \frac{\Delta x_i}{x_{\xi_i}},\\
\Delta\eta_{i,j} = \Delta\eta &= (\eta_x\Delta x)_{i,j} + (\eta_y(\Delta y + \Delta x\tan\theta))_{i,j} = \frac{\Delta y_j}{b_0 + 2b_1\eta_j} = \frac{\Delta y_j}{y_{\eta_j}},
\end{aligned} \tag{14}$$

where $x_{\xi_i} = a_0 + 2a_1\xi_i$ and $y_{\eta_j} = b_0 + 2b_1\eta_j$ for $i,j = 0,1,2,\ldots,N$.

Table 1
Truncation error coefficients in Eq. (13) in terms of their sources

	Base error	Stretching error	Skewness error	Combination error
A_1		$-\frac{1}{4}\Delta x^2(\frac{1}{Re}p + 2\cos\alpha)p$		
A_2				$-\frac{1}{2}\Delta x^2(\frac{1}{Re}p + 2\cos\alpha)p\tan\theta$
A_3		$-\frac{1}{4}\Delta y^2(\frac{1}{Re}q + 2\sin\alpha)q$		$-\frac{1}{4}\Delta x^2(\frac{1}{Re}p + 2\cos\alpha)p\tan^2\theta$ $-\frac{1}{4}\Delta y^2(\frac{1}{Re}q\tan\theta - 2\cos\alpha)q\tan\theta$
B_1	$-\frac{1}{6}\Delta x^2\cos\alpha$	$\frac{1}{3}\Delta x^2\frac{1}{Re}p$		
B_2			$-\frac{1}{2}\Delta x^2\cos\alpha\tan\theta$	
B_3			$-\frac{1}{2}\Delta x^2\cos\alpha\tan^2\theta$	$-\Delta x^2\frac{1}{Re}p\tan^2\theta - \Delta y^2\frac{1}{Re}q\tan\theta$
B_4	$-\frac{1}{6}\Delta y^2\sin\alpha$	$\frac{1}{3}\Delta y^2\frac{1}{Re}q$	$-\frac{1}{6}\Delta x^2\cos\alpha\tan^3\theta + \frac{1}{6}\Delta y^2\cos\alpha\tan\theta$	$-\frac{2}{3}\Delta x^2\frac{1}{Re}p\tan^3\theta - \frac{2}{3}\Delta y^2\frac{1}{Re}q\tan^2\theta$
C_1	$\frac{1}{12}\Delta x^2\frac{1}{Re}$			
C_2				
C_3			$-\frac{1}{2}\Delta x^2\frac{1}{Re}\tan^2\theta$	
C_4			$-\frac{2}{3}\Delta x^2\frac{1}{Re}\tan^3\theta - \frac{1}{3}\Delta y^2\frac{1}{Re}\tan\theta$	
C_5	$\frac{1}{12}\Delta y^2\frac{1}{Re}$		$-\frac{1}{4}\Delta x^2\frac{1}{Re}\tan^4\theta - \frac{1}{4}\Delta y^2\frac{1}{Re}\tan^2\theta$	

Note: $p = x_{\xi\xi}/x_\xi^2$, $q = y_{\eta\eta}/y_\eta^2$.

The error terms in Eq. (13) influence the solution with respect to both amplitude and phase. To examine the details, a solution of Eq. (12) is considered by letting $u = \phi(t)e^{i(k_x x + k_y y)}$:

$$\frac{\partial \phi}{\partial t} = -\left[i(k_x \cos\alpha + k_y \sin\alpha + \varepsilon_P) + \left(\frac{1}{Re}k_x^2 + \frac{1}{Re}k_y^2 - \varepsilon_A\right)\right]\phi, \tag{15}$$

where k_x and k_y are wavenumbers in the x and y directions, respectively, and

$$\begin{aligned} \varepsilon_P &= B_1 k_x^3 + B_2 k_x^2 k_y + B_3 k_x k_y^2 + B_4 k_y^3, \\ \varepsilon_A &= -A_1 k_x^2 - A_2 k_x k_y - A_3 k_y^2 + C_1 k_x^4 + C_2 k_x^3 k_y + C_3 k_x^2 k_y^2 + C_4 k_x k_y^3 + C_5 k_y^4. \end{aligned} \tag{16}$$

The ε_P and ε_A terms describe deviations from the exact solution in phase and amplitude in the physical domain. Coefficients of odd-derivative error terms (B_i) are related to the phase speeds of dispersion errors while their signs correspond to the directions of propagation. On the other hand, the coefficients of even-derivative terms either enhance or reduce the dissipation of the original advection–diffusion equation, and alter the amplitude of the solution. In the following subsections, the contributions of both dispersion and diffusion error terms to the numerical solution and to stability are discussed in detail.

1.1. Uniform Cartesian mesh

When a uniform Cartesian mesh is employed, the errors are reduced to their simplest and well-known forms:

$$\varepsilon_P = \varepsilon_{P(base)} = -\frac{\Delta x^2}{6}\{k_x^3 \cos\alpha\} - \frac{\Delta y^2}{6}\{k_y^3 \sin\alpha\}, \tag{17}$$

$$\varepsilon_A = \varepsilon_{A(base)} = \frac{\Delta x^2}{12}\left\{\frac{1}{Re}k_x^4\right\} + \frac{\Delta y^2}{12}\left\{\frac{1}{Re}k_y^4\right\}. \tag{18}$$

Truncation errors corresponding to the central-difference approximations of diffusion terms amplify the solution while the errors related to the advection terms do not affect the amplitude of the solution. In this baseline case, mesh spacings are the only parameters determining the dispersion and dissipation errors.

1.2. Non-uniform Cartesian mesh

Mesh stretching or compression results in amplitude and phase errors which include contributions from both advection and diffusion terms.

$$\begin{aligned} \varepsilon_P &= \varepsilon_{P(base)} + \varepsilon_{P(stretching)}, \\ \varepsilon_{P(stretching)} &= \frac{\Delta x_i^2}{3}\left\{\frac{1}{Re}p_i k_x^3\right\} + \frac{\Delta y_j^2}{3}\left\{\frac{1}{Re}q_j k_y^3\right\}, \end{aligned} \tag{19}$$

$$\begin{aligned} \varepsilon_A &= \varepsilon_{A(base)} + \varepsilon_{A(stretching)}, \\ \varepsilon_{A(stretching)} &= \frac{\Delta x_i^2}{4}\left\{\underbrace{\frac{1}{Re}p_i^2 k_x^2}_{(20)A} + \underbrace{2p_i k_x^2 \cos\alpha}_{(20)B}\right\} + \frac{\Delta y_j^2}{4}\left\{\underbrace{\frac{1}{Re}q_j^2 k_y^2}_{(20)C} + \underbrace{2q_j k_y^2 \sin\alpha}_{(20)D}\right\}, \end{aligned} \tag{20}$$

where $p_i = x_{\xi\xi}/x_{\xi_i}^2$ and $q_j = y_{\eta\eta}/y_{\eta_j}^2$. This type of mesh non-uniformity has been studied extensively and is known to a source of numerical instability [7,12,13].

Table 2
Mesh parameters for five different mapping functions

a_0	a_1	r	p
0.3	0.7	1.0083 to 1.0456	0.4925 to 14.1994
0.5	0.5	1.0067 to 1.0198	0.4504 to 3.8447
1.0	0	1.0000	0
1.5	−0.5	0.9806 to 0.9933	−3.8447 to −0.4504
1.7	−0.7	0.9564 to 0.9917	−14.1994 to −0.4925

Note: $r = \frac{x(\xi+\Delta\xi)-x(\xi)}{x(\xi)-x(\xi-\Delta\xi)}$ for $N = 100$.

A sufficient condition for maintaining the order of accuracy (second-order in this study) is that the magnitudes of p_i and q_j are bounded as x_{ξ_i} and y_{η_j} approach zero [7]. Therefore, not only the mesh stretching or compression ratio, but also the smoothness of the mesh distribution function have a significant effect on the solution quality and stability. Absolute values of non-dimensionalized p_i and q_j are roughly 0.5–14 for 0.7–4.5% of mesh stretching/compression ratio r in the examples considered in Table 2.

Figs. 3 and 4 show the phase and amplitude errors as a function of mesh skewness angle (θ) at $Re = 10^{-2}$ and 10^4, respectively. Each figure contains the total truncation error and truncation errors in terms of their sources for both stretched and compressed mesh cases. In this section, the truncation

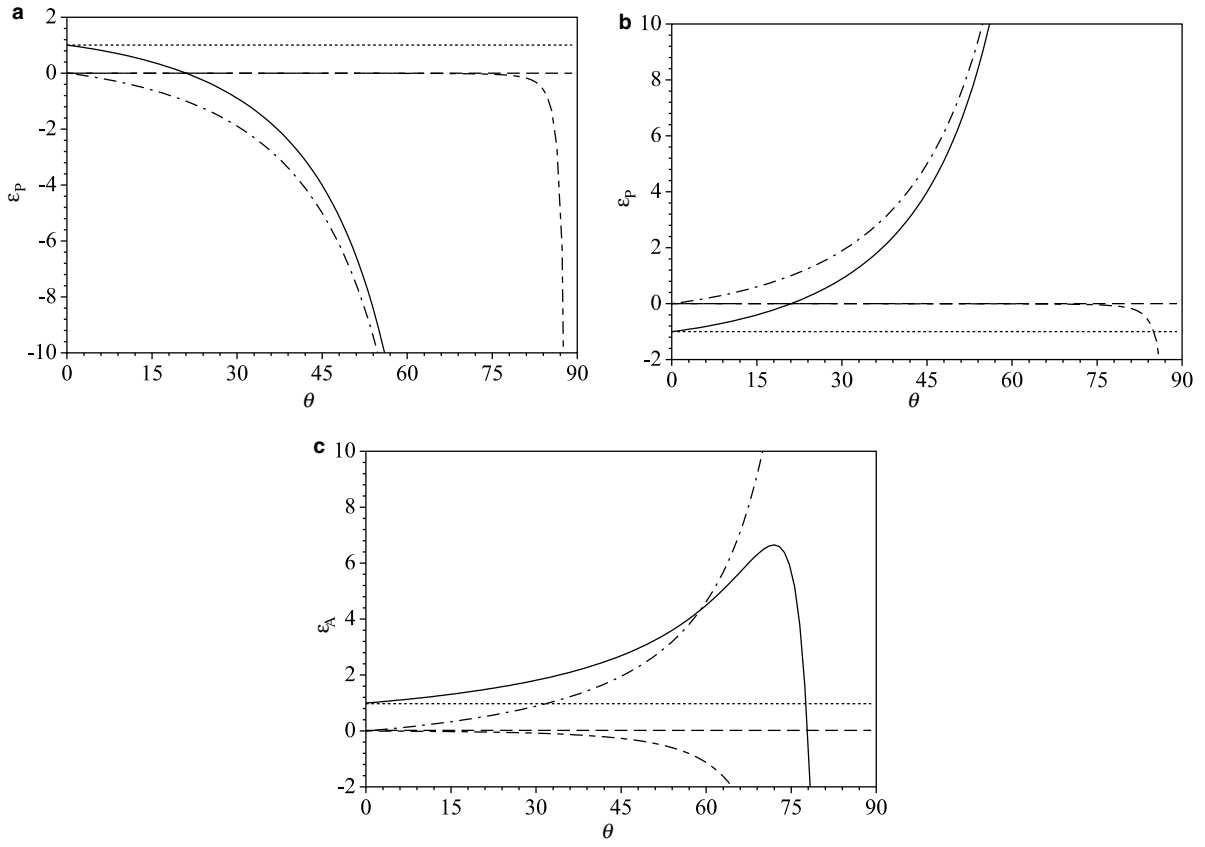

Fig. 3. Truncation errors as a function of mesh skewness angle (θ). $\alpha = \theta$, $Re = 10^{-2}$, $\Delta x = \Delta y$, and $k_x = k_y = 1$ are used: (a) phase error in case of $p = 3.84$; (b) phase error in case of $p = -3.84$; (c) amplitude error in case of $p = \pm 3.84$. —, total error; ----, base error; ···, stretching error; –··–, skewness error; –·–, combination error. Errors are normalized with the total error at $\theta = 0°$.

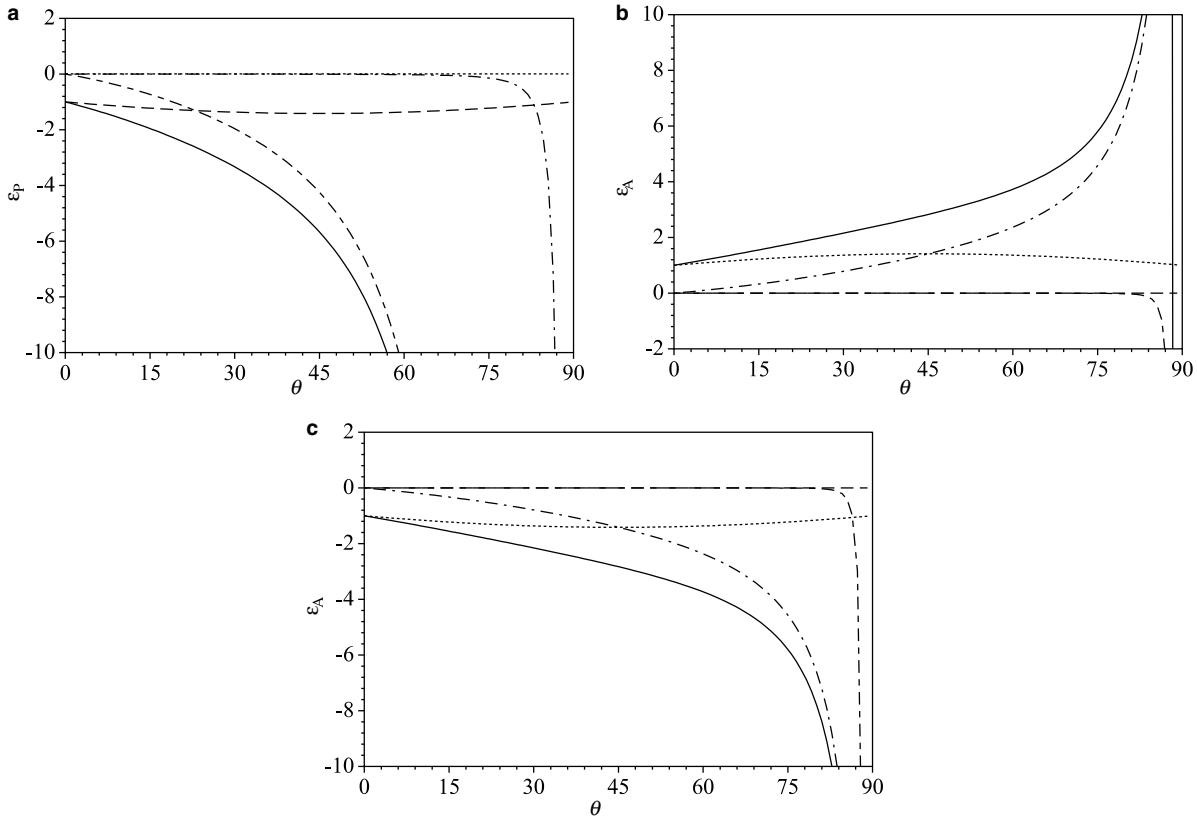

Fig. 4. Truncation errors as a function of mesh skewness angle (θ). $\alpha = \theta, Re = 10^4$, $\Delta x = \Delta y$, and $k_x = k_y = 1$ are used: (a) phase error in case of $p = 3.84$; (b) amplitude error in case of $p = 3.84$; (c) amplitude error in case of $p = -3.84$. —, total error; ----, base error; $\cdots$, stretching error; – – –, skewness error; – · –, combination error. Errors are normalized with the total error at $\theta = 0°$.

errors related to the mesh stretching/compression are discussed, and other curves will be discussed in Sections 1.3 and 1.4.

In the diffusion-dominated case, the phase errors associated with mesh stretching/compression propagate in opposite directions depending on signs of p_i and q_j for given k_x and k_y ($\cdots$ in Figs. 3(a) and (b)). The amplitude errors cause a reduction in the effective viscosity in Eq. (9), and hence amplify the solution in time for both stretching and compression cases (see error terms (20)A and (20)C in Eq. (20) and $\cdots$ in Fig. 3(c)).

If the viscosity is negligible, the effect of mesh non-uniformity is only significant for amplitude errors ($\cdots$ in Figs. 4(b) and (c)). Amplification or damping of the solution is determined by the signs of error terms (20)B and (20)D. This can cause the non-physical deformation of a vortex propagating through a non-uniform mesh region at a high Reynolds number. A highly stretched mesh ($p_i \cos\alpha > 0$ and $q_j \sin\alpha > 0$) is also responsible for numerical instability by enhancing amplification errors ($\cdots$ in Fig. 4(b)). Similar observations were made by Cain and Bush [12].

1.3. Uniform skewed mesh

As observed in the uniform Cartesian mesh case, advection terms only modulate phase errors while diffusion terms are responsible for amplitude errors. However, the characteristics of both errors are strongly affected by the tangent functions of skewness angle (θ).

$$\varepsilon_{\mathrm{P}} = \varepsilon_{\mathrm{P(base)}} + \varepsilon_{\mathrm{P(skewness)}},$$
$$\varepsilon_{\mathrm{P(skewness)}} = \underbrace{\left\{-\frac{\Delta x^2}{6}k_y^3\cos\alpha\right\}\tan^3\theta}_{(21)A} + \{\cdots\}\tan^2\theta + \cdots, \tag{21}$$

$$\varepsilon_{\mathrm{A}} = \varepsilon_{\mathrm{A(base)}} + \varepsilon_{\mathrm{A(skewness)}},$$
$$\varepsilon_{\mathrm{A(skewness)}} = \underbrace{\left\{-\frac{\Delta x^2}{4}\frac{1}{Re}k_y^4\right\}\tan^4\theta}_{(22)A} + \{\cdots\}\tan^3\theta + \cdots. \tag{22}$$

For skewness angles greater than 45°, the error terms (21)A and (22)A dominate other error terms because of the $\tan^3\theta$ and $\tan^4\theta$ factors, respectively. On the other hand, magnitudes of the error terms are rapidly reduced as θ approaches zero.

The most notable feature in the skewness related errors is the excessive dissipation ((22)A). The numerical dissipation is a peculiar aspect of mesh skewness errors since it is non-existent in central-difference schemes on a Cartesian mesh (see Sections 1.1 and 1.2) except for the region of high mesh compression ($\cdots$ in Fig. 4(c)). The numerical dissipation is especially notable in the case of small Re (–·– in Fig. 3(c)) while the numerical dissipation is not significant except for an impractical skewness angle ($\theta \gg 80°$) in the case of high Re (–··– in Figs. 4(b) and (c)). On the other hand, as seen in Fig. 4(a) (–·–), the mesh skewness significantly enhances the phase error in the high Re case while the phase error is not significant in the diffusion-dominated case.

Therefore, if a uniform (or mildly non-uniform) skewed mesh is employed, the excessive numerical dissipation will deteriorate the solution in the case of low Reynolds number, while the enhanced numerical dispersion will be a main concern in the high Reynolds number case.

1.4. Non-uniform skewed mesh

All error terms in Eq. (13) or in Table 1 are present on a non-uniform skewed mesh. More drastic effects on both phase and amplitude errors can be induced by the combination of mesh stretching/compression and skewness

$$\varepsilon_{\mathrm{P}} = \varepsilon_{\mathrm{P(base)}} + \varepsilon_{\mathrm{P(stretching)}} + \varepsilon_{\mathrm{P(skewness)}} + \varepsilon_{\mathrm{P(combined)}},$$
$$\varepsilon_{\mathrm{P(combined)}} = \underbrace{\left\{-\frac{2\Delta x_i^2}{3}\frac{1}{Re}q_j k_y^3\right\}\tan^3\theta}_{(23)A} + \{\cdots\}\tan^2\theta + \cdots, \tag{23}$$

$$\varepsilon_{\mathrm{A}} = \varepsilon_{\mathrm{A(base)}} + \varepsilon_{\mathrm{A(stretching)}} + \varepsilon_{\mathrm{A(skewness)}} + \varepsilon_{\mathrm{A(combined)}},$$
$$\varepsilon_{\mathrm{A(combined)}} = \underbrace{\left\{\frac{\Delta x_i^2}{4}\frac{1}{Re}p_i^2k_y^2 + \frac{\Delta y_j^2}{4}\frac{1}{Re}q_j^2k_y^2\right\}\tan^2\theta}_{(24)A} + \underbrace{\left\{\frac{\Delta x_i^2}{2}p_i k_y^2\cos\alpha\right\}\tan^2\theta}_{(24)B} + \{\cdots\}\tan\theta. \tag{24}$$

The combined effect of mesh non-uniformity and skewness on the phase errors is induced by the discretization of viscous terms. With moderate to high viscosity, phase errors are dominated by the (23)A term which propagate in opposite direction depending on the sign of q_j (–·– in Figs. 3(a) and (b)). In an advection-dominated case, as shown in Section 1.3, the total dispersion error is characterized by the error terms generated from the discretization of advection terms (Eq. (21)).

Both the combination error (24)A and the skewness only error (22)A are important in the viscous-dominated case, and they result in amplification of the solution except for a very large skewness angle ($\theta > 78°$ in the case considered in Fig. 3(c), see — and –·– for total and combination amplitude errors). However, in the advection-dominated case, the error term (24)B becomes the dominant one. This error also appears as either amplification or damping effects depending on the convection velocity $\tilde{C}^x (= \cos\alpha)$ and mesh stretching parameter p_i. For instance, mesh stretching ($p_i \cos\alpha > 0$) causes a significant amplification of error which can lead to numerical instability (–·– in Fig. 4(b)). In contrast, mesh compression ($p_i \cos\alpha < 0$) results in enhanced dissipation by the factor of $\tan^2\theta$ (–·– in Fig. 4(c)).

In addition to the non-uniform Cartesian mesh case where mesh stretching results in enhanced amplification (see Section 1.2), a stretched and highly skewed mesh further enhances amplification error and promotes numerical instability. This situation is often encountered in the vortex shedding from the trailing edge of a turbine or compressor blade (see Fig. 1 and [1,2]). From this perspective, the meshes employed by Wu and Durbin [14] and Mittal et al. [2] were able to avoid skewness in the wake region similar to the one considered in Fig. 1(b).

Interestingly, numerical instability in the blade boundary layer was less severe or non-existent even though mesh skewness angles are quite large in the example considered in Fig. 1 ($\theta_{\max} = 57°$) and in the simulation of Wu and Durbin [14] ($\theta_{\max} = 63.2°$). In both cases, the streamwise mesh stretching ratios in the blade region are much smaller than those in the wake region. Therefore, in the high Reynolds number case, the amplitude error terms (20)A, (20)C, and (24)A become negligible. In addition, unlike the unsteady convecting vortex structures in the wake, the flow in the boundary layer is predominantly aligned to one set of grid lines. This indicates that numerical instability noted in the present study may be caused by not only the numerical scheme and mesh skewness but also the characteristics of the flow and grid resolution. This feature will be further discussed in Section 2.4.

The present truncation error analysis also explains the findings of Armenio and Piomelli [15]. They performed large-eddy simulation of a plane turbulent channel flow employing both Cartesian and skewed meshes, and obtained similar results in both cases. Since they used a uniform mesh spacing in the streamwise direction, the particularly detrimental effect of combining mesh skewness with stretching/compression was not present.

2. Modified wavenumber analysis

The truncation error analysis revealed how mesh stretching and skewness affect the quality of the numerical solution in terms of phase and amplitude errors. However, the analysis was limited to the spatial-discretization errors in a semi-discretized equation, since the inclusion of at least second-order time discretization makes the analysis very complicated. On the other hand, the modified wavenumber analysis allows a quantitative investigation of the effects of mesh skewness on the solution quality and also on the temporal stability of the solution method in the transformed computational domain.

In interpreting the results of the present modified wavenumber analysis, it should be noted that the errors and stability of the solution method are determined in the computational coordinates (ξ, η). Therefore, the absolute magnitudes and relative variations of the errors different in the physical domain (x, y). However, since the actual computation is performed in the transformed coordinates, it is more meaningful to discuss the stability limit of time-integration in those coordinates.

By assuming a solution of the following form:

$$u(\xi, \eta, t) = \phi(t) e^{i(k_\xi \xi + k_\eta \eta)}, \tag{25}$$

the partial differential equation (10) becomes an ordinary differential equation

$$\frac{\mathrm{d}\phi(t)}{\mathrm{d}t} = \lambda\phi(t), \tag{26}$$

where

$$\begin{aligned}\lambda &= -\mathrm{i}\left(\xi_x k_\xi \cos\alpha + \eta_x k_\eta \cos\alpha + \eta_y k_\eta \sin\alpha - \frac{1}{Re}(\xi_{xx}k_\xi + \eta_{xx}k_\eta + \eta_{yy}k_\eta)\right)\\ &\quad - \frac{1}{Re}(\xi_x^2 k_\xi^2 + 2\xi_x\eta_x k_\xi k_\eta + \eta_x^2 k_\eta^2 + \eta_y^2 k_\eta^2)\\ &= -\mathrm{i}\left(\frac{\cos\alpha}{\Delta x_i}(k_\xi\Delta\xi) + \frac{(\tan\alpha - \tan\theta)\cos\alpha}{\Delta y_j}(k_\eta\Delta\eta)\right) - \mathrm{i}\frac{1}{Re}\left(\frac{p_i}{\Delta x_i}(k_\xi\Delta\xi) + \frac{q_j\tan\theta(\tan\theta - 1)}{\Delta y_j}(k_\eta\Delta\eta)\right)\\ &\quad - \frac{1}{Re}\left(\frac{1}{\Delta x_i^2}(k_\xi\Delta\xi)^2 - \frac{2\tan\theta}{\Delta x_i\Delta y_j}(k_\xi\Delta\xi)(k_\eta\Delta\eta) + \frac{1+\tan^2\theta}{\Delta y_j^2}(k_\eta\Delta\eta)^2\right).\end{aligned} \tag{27}$$

Finite-difference approximations of the spatial derivatives replace wavenumbers k_ξ and k_η in Eq. (27) with modified wavenumbers. Modified wavenumbers corresponding to the second-order central-difference approximations of the first and second derivatives are

$$\begin{aligned}k_\xi^{1C} &= \frac{\sin(k_\xi\Delta\xi)}{\Delta\xi},\\ k_\eta^{1C} &= \frac{\sin(k_\eta\Delta\eta)}{\Delta\eta},\\ k_\xi^{2C} &= \frac{2(1-\cos(k_\xi\Delta\xi))}{\Delta\xi^2},\\ k_\eta^{2C} &= \frac{2(1-\cos(k_\eta\Delta\eta))}{\Delta\eta^2},\end{aligned} \tag{28}$$

in the ξ and η directions.

For comparison, the modified wavenumbers for the second-order upwind approximations of the first derivatives,

$$\begin{aligned}k_\xi^{1U} &= \frac{(\mathrm{sign}_\xi)\mathrm{i}(3 - 4\cos(k_\xi\Delta\xi) + \cos(2k_\xi\Delta\xi)) + (4\sin(k_\xi\Delta\xi) - \sin(2k_\xi\Delta\xi))}{2\Delta\xi},\\ k_\eta^{1U} &= \frac{(\mathrm{sign}_\eta)\mathrm{i}(3 - 4\cos(k_\eta\Delta\eta) + \cos(2k_\eta\Delta\eta)) + (4\sin(k_\eta\Delta\eta) - \sin(2k_\eta\Delta\eta))}{2\Delta\eta},\end{aligned} \tag{29}$$

are also considered, where

$$\begin{aligned}&\mathrm{sign}_\xi = - \quad \text{for } \xi_x\cos\alpha > 0,\\ &\mathrm{sign}_\xi = + \quad \text{for } \xi_x\cos\alpha < 0,\\ &\mathrm{sign}_\eta = - \quad \text{for } \eta_x\cos\alpha + \eta_y\sin\alpha > 0,\\ &\mathrm{sign}_\eta = + \quad \text{for } \eta_x\cos\alpha + \eta_y\sin\alpha < 0.\end{aligned} \tag{30}$$

The modified wavenumbers, $k_{\xi(\eta)}^{1C}$ and $k_{\xi(\eta)}^{1U}$, are compared in Fig. 5. Distinct features of modified wavenumbers also influence the global properties of the discretized ordinary-differential equation (Eq. (26)). Note that the modified wavenumber of second-order central-difference does not introduce imaginary values, while the upwind scheme shows a dissipative feature, especially at high wavenumbers (Fig. 5(b)). The present analysis can also be extended to other spatial-discretization methods including compact schemes.

For a quantitative analysis, a two-dimensional wavenumber space is constructed by discretizing the domain of $-\pi \leqslant k_\xi\Delta\xi, k_\eta\Delta\eta \leqslant \pi$ with 360 equal intervals in both directions. In this domain, the wavenumbers

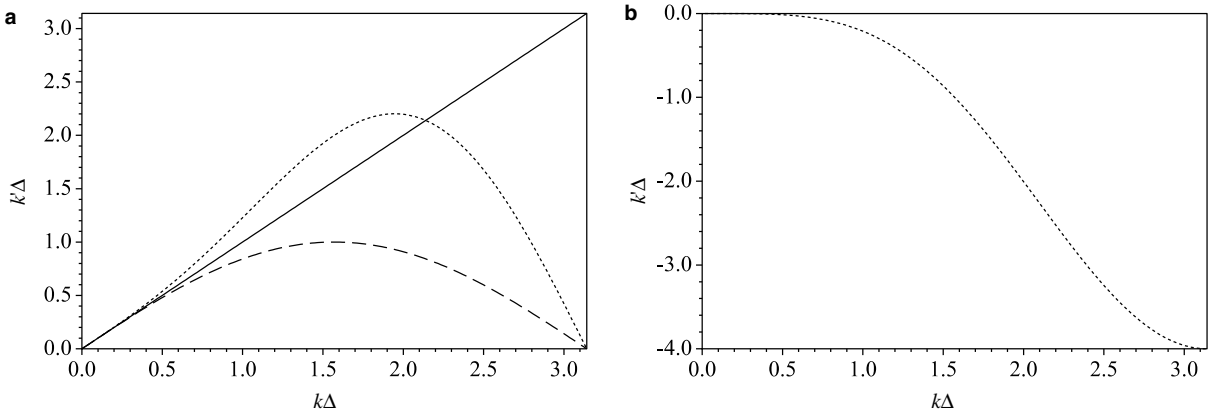

Fig. 5. (a) Real parts and (b) imaginary parts of modified wavenumbers. —, exact (spectral); ----, second-order central-difference; ···, second-order upwind-difference. — and ---- are coincident with the line of $k'\Delta = 0$ in (b).

k_ξ and k_η are used to represent a spectral (exact) solution, while they are replaced with modified wavenumbers to represent finite-difference approximations. Advection terms are approximated by either central- or upwind-differences, and diffusion terms including cross-derivative terms are approximated by central difference.

2.1. Mesh skewness effects on numerical errors

The numerical errors associated with spatial discretizations on a skewed mesh are considered in a location of $\Delta x_i = \Delta y_j = \Delta$ in Eq. (27) where $p_i (= q_j)$ and Δ are set to 3.84 and 5.05×10^{-3} which correspond to the mesh stretching ratio $r = 2\%$ in the considered mapping function (see the second set of mesh parameters in Table 2). Eq. (27) is rewritten in this location as

$$\begin{aligned}\lambda\Delta t = &-\mathrm{i}sPe^x((k_\xi\Delta\xi) + (\tan\alpha - \tan\theta)(k_\eta\Delta\eta)) - \mathrm{i}sp_i\Delta((k_\xi\Delta\xi) + \tan\theta(\tan\theta - 1)(k_\eta\Delta\eta)) \\ &- s((k_\xi\Delta\xi)^2 - 2\tan\theta(k_\xi\Delta\xi)(k_\eta\Delta\eta) + (1 + \tan^2\theta)(k_\eta\Delta\eta)^2),\end{aligned} \tag{31}$$

where $Pe^x = \tilde{C}^x Re\Delta = Re\Delta\cos\alpha$ and $s = \Delta t/(Re\Delta^2)$.

In Fig. 6, the real parts of the differences between the numerical and exact values of $\lambda\Delta t/s$ (defined in Eq. (31)) are shown. The numerical values are computed using modified wavenumbers for discretizations on a Cartesian mesh ($\theta = 0$) with flow direction $\alpha = 45°$ and $Re = 10^4$ (or $Pe^x = 35.7$) (see Fig. 2 for definitions of θ and α). Two different methods of discretization are considered: a second-order central-difference scheme for both advection and diffusion terms (henceforth denoted CD2), and a hybrid scheme consisting of second-order upwinding for advection terms and second-order central-differencing for diffusion terms (henceforth UD2).

In this Cartesian mesh, compared to the exact values, CD2 shows amplifications of solution which are enhanced in the high wavenumber regions (Fig. 6(a)). On the contrary, as shown in Fig. 6(b), UD2 produces enhanced dissipation. The amplitude error characteristics of CD2 is dramatically changed when a highly skewed mesh is employed. Fig. 7 depicts the differences between the numerical approximations and exact values of $\lambda\Delta t/s$ for a skewed mesh with $\theta = 60°$, $\alpha = 45°$, and $Re = 10^4$. Unlike the Cartesian mesh case, CD2 on a skewed mesh introduces dissipation errors in the lower left and upper right regions of wavenumber space as shown in Fig. 7(a). The numerical dissipation even in a stretched mesh is a peculiar aspect of mesh skewness related errors since it is usually non-existent in central-difference schemes in a Cartesian mesh. On the other hand, similar to the Cartesian mesh case, UD2 suffers from excessive numerical dissipation in a highly skewed mesh (Fig. 7(b)).

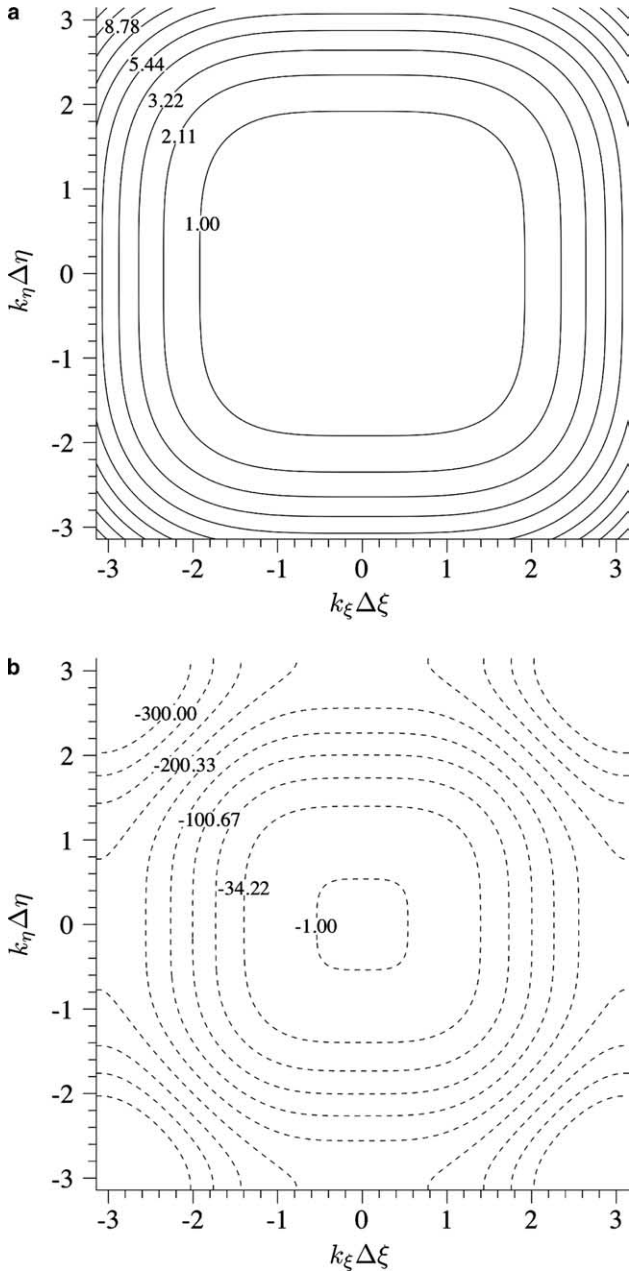

Fig. 6. Real parts of $(\lambda \Delta t/s)_{\text{numerical}} - (\lambda \Delta t/s)_{\text{exact}}$ in wavenumber space at $\theta = 0°$, $\alpha = 45°$, and $Re = 10^4$. (a) CD2; (b) UD2.

In a highly skewed mesh, the central differencing is still preferred to the upwind differencing due to its less dissipative feature which is particularly important in the large-eddy simulation of turbulent flow. As will be discussed in Section 1.3, the use of the central differencing is advantageous in terms of allowable maximum time-step size. The highly enhanced amplitude errors accompanying from the use of the upwind differencing lead to a significantly reduced allowable time-step size.

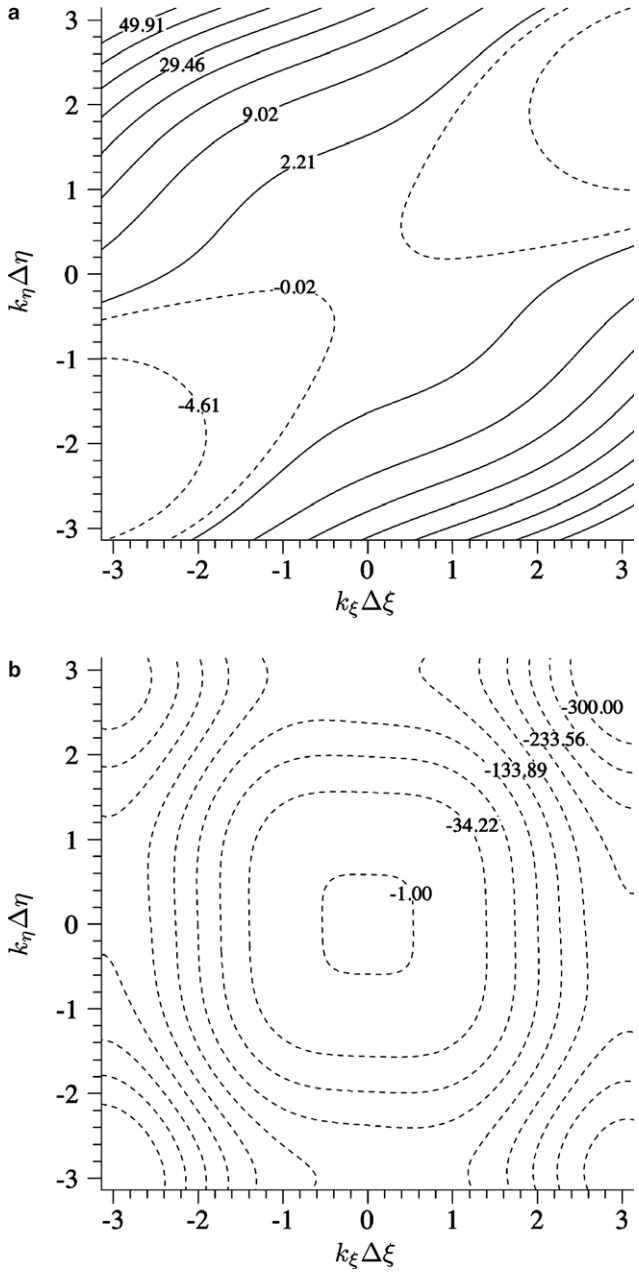

Fig. 7. Real parts of $(\lambda \Delta t/s)_{\text{numerical}} - (\lambda \Delta t/s)_{\text{exact}}$ in wavenumber space at $\theta = 60°$, $\alpha = 45°$, and $Re = 10^4$. (a) CD2; (b) UD2.

2.2. Mesh skewness effects on the cell Peclet number

Applying the first-order Euler explicit time-integration method and second-order central-difference scheme to Eq. (26), and assuming a uniform skewed mesh of $\Delta x = \Delta y = \Delta$ and $p_i = 0$ in Eq. (31), results in the following amplification factor:

$$1+\lambda\Delta t = -\mathrm{i}\{sPe^{x}(\sin\phi+(\tan\alpha-\tan\theta)\sin\gamma)\}+\{1-2s(1-\cos\phi-\tan\theta\sin\phi\sin\gamma +(1+\tan^2\theta)(1-\cos\gamma))\}, \tag{32}$$

where $\phi = k_\xi\Delta\xi$ and $\gamma = k_\eta\Delta\eta$, respectively. For a stable solution, $|1+\lambda\Delta t|\leqslant 1$ needs to be satisfied. This constraint gives:

$$0<s\leqslant\frac{1}{Y_{\max}},\quad 0<Pe^{x2}\leqslant\frac{4Y(1-sY)}{sX^2}, \tag{33}$$

where

$$\begin{aligned} X &= \sin\phi+(\tan\alpha-\tan\theta)\sin\gamma,\\ Y &= 1-\cos\phi-\tan\theta\sin\phi\sin\gamma+(1+\tan^2\theta)(1-\cos\gamma). \end{aligned} \tag{34}$$

For instance, in the non-skewed, uniform mesh ($\theta = 0$) case with $\alpha = 45°$, we obtain the well-known results for a linear convection–diffusion equation [16]:

$$0<s\leqslant\frac{1}{4},\quad 0<Pe^{x2}\leqslant 4. \tag{35}$$

Fig. 8 shows the maximum allowable Peclet numbers (Pe^x) and time-step sizes (s) as a function of mesh skewness angle for two sets of convection velocities, $\alpha = 45°$ and $\alpha = -45°$. Regardless of the flow direction, the maximum allowable viscous time-step size s decreases with the mesh skewness angle. In general, the allowable Peclet number also decreases with the mesh skewness angle when it is greater than 45°. From the relation $\mathrm{CFL} = \tilde{C}\Delta t/\Delta = s\times Pe$, the convective time-step also decreases with the mesh skewness angle. Furthermore, the maximum allowable Peclet number shows a dependence on the flow direction. This suggests that in addition to mesh parameters, the flow direction also affects the stability of the numerical scheme. This issue will be further discussed in Section 1.4.

2.3. Mesh skewness effects on time-integration schemes

In this section, the temporal stability of the numerical approximations of the governing equation and its dependence on the mesh skewness angle are discussed. In general, large mesh skewness limits the allowable

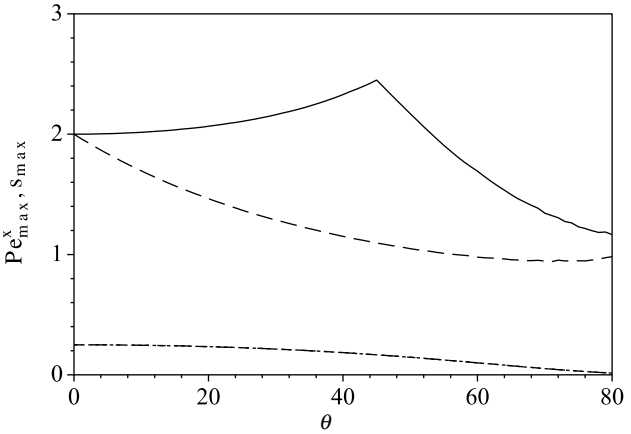

Fig. 8. Maximum allowable $s = \Delta t/(Re\Delta^2)$ and Peclet number as a function of mesh skewness angle (θ). —, $Pe^x_{\max}$ for $\alpha = 45°$; ----, $Pe^x_{\max}$ for $\alpha = -45°$; ⋯, $s_{\max}$ for $\alpha = 45°$; – – –, $s_{\max}$ for $\alpha = -45°$ in Eq. (32). ⋯ and – – – are identical.

time-step size due to increased discretization errors and enhanced magnitude of amplification factor. This issue is examined employing a third-order Runge–Kutta time-integration method.

The stability of a third-order Runge–Kutta scheme (RK3) is determined using the amplification factor [17]:

$$\sigma = 1 + \lambda\Delta t + \frac{(\lambda\Delta t)^2}{2} + \frac{(\lambda\Delta t)^3}{6}, \tag{36}$$

where for stable solutions, the condition $|\sigma| \leqslant 1$ must be satisfied. Fig. 9 shows the variation of the maximum allowable time-step size (s) with θ variation for three different values of Re ($\sqrt{2}$, $10^2\sqrt{2}$, and $10^4\sqrt{2}$) when α is set to 45°. In the small to moderate values of Re, the maximum time-step sizes are reduced with increasing skewness angle θ (Figs. 9(a) and (b)). In those cases, for a given skewness angle, the allowable time-step sizes are in the order of CD2, UD2, and spectral methods. In the advection-dominated case, the peak allowable s is found in the skewness angle (θ) around the flow direction (α) (Fig. 9(c)) and, for a given skewness angle, CD2 leads to a higher allowable time-step size than UD2 and spectral schemes.

Other explicit time-integration methods such as the second-order Runge–Kutta (RK2) and second- and third-order Adams–Bashforth schemes (AB2 and AB3) have also been considered. In those schemes, the variation in the allowable time-step size as a function of mesh skewness angle is similar to that in RK3, and the values of allowable time-step sizes are found in the order of RK3, RK2, AB2, and AB3 for a given skewness angle.

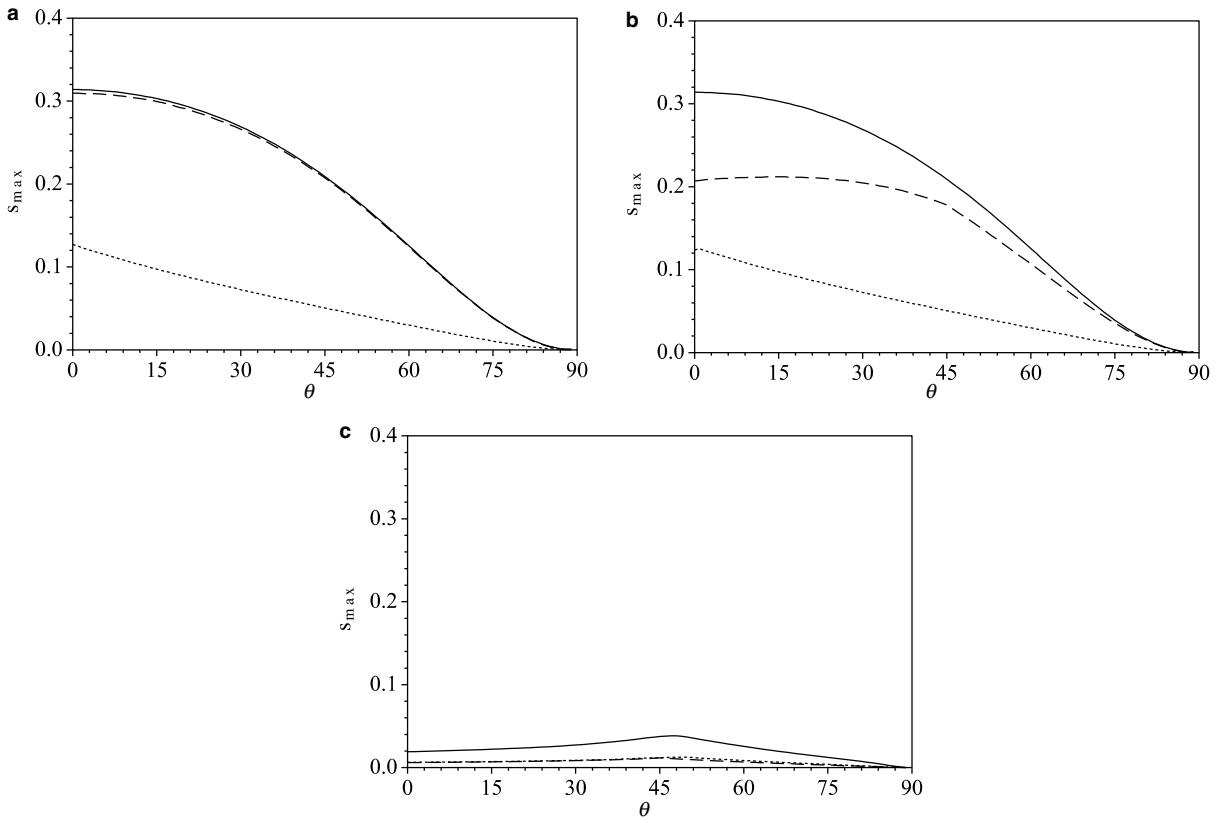

Fig. 9. Maximum allowable $s = \Delta t/(Re\Delta^2)$ as a function of mesh skewness angle (θ) when a third-order Runge–Kutta scheme is used with $\alpha = 45°$. (a) $Re = \sqrt{2}$; (b) $Re = 10^2$; (c) $Re = 10^4\sqrt{2}$. —, CD2; ----, UD2; ···, exact (spectral).

The present analysis also has implications for large-eddy simulation of turbulent flow on a highly skewed mesh. When an eddy-viscosity type subgrid-scale model is used, the ratio of instantaneous, local eddy-viscosity to the molecular viscosity can reach $O(10^3$–$10^4)$. In such cases, the allowable time-step (Δt_{max}) experiences a sudden drop due to the enhanced effective viscosity since $\Delta t = sRe\Delta^2$. This problem is further exacerbated when a highly skewed mesh is employed. For example, at $\theta = 50°$, Δt is reduced from $370\Delta^2$ for $Re = 10^4\sqrt{2}$ (Fig. 9(c)) to $18\Delta^2$ for $Re = 10^2\sqrt{2}$ (Fig. 9(b)). Therefore, when mesh skewness is indispensable, a fully implicit time-integration method is highly preferred.

2.4. Flow direction and mesh skewness

In Section 1.3, the case in which the grid is skewed to a fixed flow direction ($\alpha = 45°$) was considered. In this section, the effects of flow direction for a fixed skewness angle on the allowable time-step size and on the numerical errors are investigated.

The allowable time-step sizes of numerical schemes are significantly altered by the change of flow direction. Fig. 10 shows the maximum allowable time-step size s as a function of flow direction α when a third-order Runge–Kutta scheme is used with a fixed mesh skewness angle $\theta = 50°$ and $Re = 10^4$. As already found in the previous section, CD2 (—) allows a higher time-step size than UD2 (----) and spectral ($\cdots$) methods for a given flow direction. The local maximum time-step size is obtained when the flow direction is aligned to the mesh lines.

Figs. 11(a) and (b) show the variations of errors in both real and imaginary parts of $\lambda\Delta t/s$ as a function of flow direction. As shown in Fig. 11(a), in this case, the amplitude errors obtained from CD2 are invariant to the flow direction (— and ---- lines). In contrast, UD2 shows sensitivity to the variation of flow direction (α), where the local minimum in dissipation errors occur when the flow direction is aligned to the mesh lines ($\cdots$ and – – – lines). As discussed in Section 1.1, the present skewness angle ($\theta = 50°$) also produces dissipation errors for a range of wavenumbers in CD2 (for example, — in Fig. 11(a)), however, these errors are much smaller than those in UD2. In contrast to the real part of λ, CD2 shows high sensitivity of the imaginary part of λ to the variation of flow direction. UD2 results in similar magnitudes of phase errors to those in CD2.

The situation considered here is often observed in real flows, in which a vortex is convected through a skewed mesh region. The present analysis suggests that the phase errors in CD2 may introduce different wave speeds, thereby generating a non-physical distortion of vortex shape. On the other hand, UD2

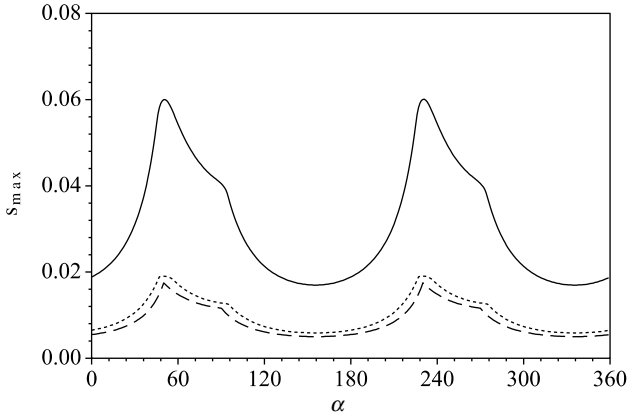

Fig. 10. Maximum allowable $s = \Delta t/(Re\Delta^2)$ as a function of flow direction (α) when a third-order Runge–Kutta scheme is used with $\theta = 50°$ and $Re = 10^4$. —, CD2; ----, UD2; $\cdots$, exact (spectral).

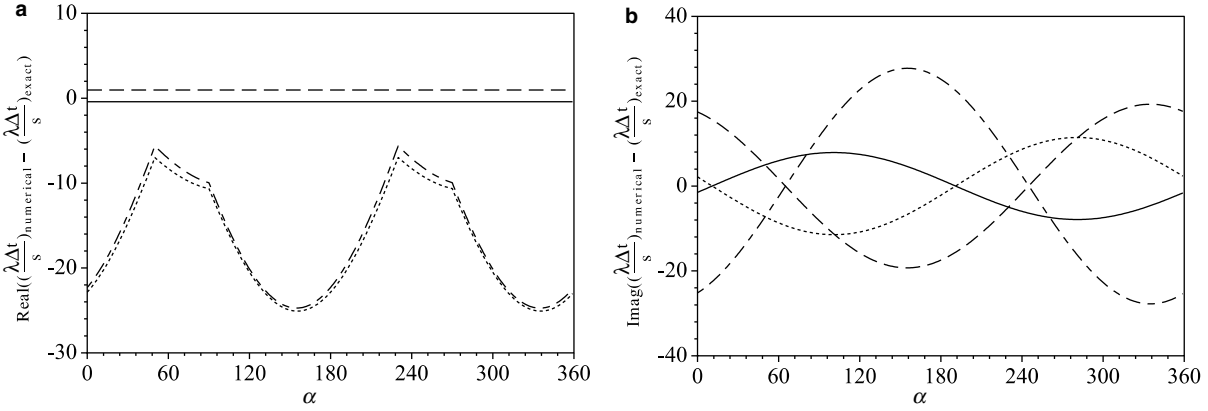

Fig. 11. Real and imaginary parts of $(\lambda\Delta/s)_{\mathrm{numerical}} - (\lambda\Delta t/s)_{\mathrm{exact}}$ as a function of flow direction (α) with a fixed mesh skewness angle ($\theta = 50°$) and $Re = 10^4$. (a) Real part; (b) imaginary part. —, CD2 for $(k_\xi\Delta\xi, k_\eta\Delta\eta) = (1,1)$; ----, CD2 for $(k_\xi\Delta\xi, k_\eta\Delta\eta) = (1,-1)$; ···, UD2 for $(k_\xi\Delta\xi, k_\eta\Delta\eta) = (1,1)$; – – –, UD2 for $(k_\xi\Delta\xi, k_\eta\Delta\eta) = (1,-1)$.

introduces amplitude errors which are dependent on the flow direction and thereby causes a non-physical distortion of vortex strength as well as the shape.

3. Summary

The effects of mesh non-uniformity and skewness on numerical flow simulations have been studied in detail using the advection–diffusion equation as a model for the Navier–Stokes equations. Truncation error and modified wavenumber analyses of this equation reveal the influence of mesh non-uniformity and skewness on the numerical accuracy and stability.

The current model equation does not include the pressure gradient term and its associated effects. However, within the context of the current analyses, the primary effect of the pressure gradient is expected to be an acceleration or deceleration in the fluid velocity, leading to a spatially varying value of the convection velocity (C). This is not expected to fundamentally change the conclusions of the current study since the analyses are local in nature where the assumption of a constant convection speed is still valid. Also, excluded from the current analyses are issues of discrete mass, momentum and energy conservation. In general, schemes that conserve these quantities discretely such as those in [18–21] are preferable over those that are not strictly conservative. However, even these conservative schemes are subject to truncation errors and spurious effects of the type discussed in the current paper.

The key findings of the present truncation error and modified wave number analyses can be summarized as follows:

- Although the central-difference scheme is dissipation-free on a uniform Cartesian mesh, on a uniform skewed mesh, it exhibits large numerical dissipation in the low Reynolds number case while numerical dispersion is a major concern in the high Reynolds number case.
- The amplification error and resulting numerical instability are further enhanced if mesh skewness is coupled with mesh stretching.
- The numerical instability encountered in actual computations on a highly skewed mesh can be explained by the present analysis. The mesh stretching ratio needs to be reduced as the mesh skewness angle increases.

- The temporal stability of numerical schemes is highly affected by the mesh skewness. The maximum allowable time-step size is reduced because of increased discretization errors and enhanced amplification factor.
- The angle between mesh lines and flow direction also affects numerical errors and stability.

The robustness of the central-difference scheme in terms of amplitude errors, compared to the upwind schemes, is quite noticeable when the flow direction is varied for a fixed mesh skewness angle. The central-differencing shows insensitivity of the amplitude error to the flow direction. When a highly skewed mesh is employed, the maximum allowable time-step size is achievable by aligning one set of mesh lines parallel to the flow direction.

The numerical characteristics of central-difference schemes relative to upwind schemes on a skewed mesh is quantitatively the same as on a Cartesian mesh. In general, central-differencing shows significantly lower dissipation than upwind-differencing, although it tends to exhibit larger dispersion errors. The low dissipative features are especially important in the large-eddy simulation of turbulent flow. Therefore, in relative terms, the central-difference scheme is still preferred to the upwind-difference scheme on a significantly skewed mesh judged by the amplitude errors and the allowable time-step size.

The present study further suggests that a sufficiently refined mesh capable of resolving the important flow scales is needed when a highly skewed mesh is employed since the amplitude errors at high wavenumbers significantly enhanced by the mesh skewness. Finally, in a highly skewed mesh system, the allowable time-step size experiences a severe reduction when an explicit time-integration method is employed. Therefore, an implicit time-integration method is more suitable.

Acknowledgments

The authors acknowledge the support of the Office of Naval Research under Grant No. N00014-99-1-0389, with Dr. Ki-Han Kim as program manager. Computer time was provided by a Challenge Project Grant (C82) from the US Department of Defense (DoD) High Performance Computing Modernization Program (HPCMP) through Army Research Laboratory (ARL) Major Shared Resource Center (MSRC).

References

[1] D. You, R. Mittal, M. Wang, P. Moin, Large-eddy simulation of a rotor tip-clearance flow, AIAA Paper 2002-0981, 2002.
[2] R. Mittal, S. Venkatasubramanian, F.M. Najjar, Large eddy simulation of flow through a low-pressure turbine, AIAA Paper 2001-2560, 2001.
[3] M. Wang, P. Moin, Computation of trailing-edge flow and noise using large-eddy simulation, AIAA Journal 38 (2000) 2201–2209.
[4] C. Hah, A numerical modeling of endwall and tip-clearance flow of an isolated compressor rotor, Journal of Engineering for Gas Turbines and Power 108 (1986) 15–21.
[5] S.E. Gorrell, T.H. Okiishi, W.W. Copenhaver, Stator–rotor interactions in a transonic compressor – part 2: description of a loss-producing mechanism, Journal of Turbomachinery 125 (2003) 336–345.
[6] T.H. Fransson, M. Jöcker, A. Böles, P. Ott, Viscous and inviscid linear/nonlinear calculations versus quasi-three-dimensional experimental cascade data for a new aeroelastic turbine standard configuration, Journal of Turbomachinery 121 (1999) 717–725.
[7] J.F. Thompson, Z.U.A. Warsi, C.W. Mastin, Numerical Grid Generation: Foundation and Applications, North-Holland, Amsterdam, 1985.
[8] D. Lee, Y.M. Tsuei, A formula for estimation of truncation errors of convection terms in a curvilinear coordinate system, Journal of Computational Physics 98 (1992) 90–100.
[9] S. Sankaranarayanan, M.L. Spaulding, A study of the effects of grid non-orthogonality on the solution of shallow water equations in boundary-fitted coordinate systems, Journal of Computational Physics 184 (2003) 299–320.
[10] H. Shi, J.L. Drewniak, Dispersion comparison for DSI- and tensor-based nonorthogonal FDTD, IEEE Microwave and Guided Wave Letters 6 (5) (1996) 193–195.

[11] F. Xiao, H. Yabe, Numerical dispersion relation for FDTD method in general curvilinear coordinates, IEEE Microwave and Guided Wave Letters 7 (2) (1997) 48–50.
[12] A.B. Cain, R.H. Bush, Numerical wave propagation analysis for stretched grids, AIAA Paper 94-0172, January, 1994.
[13] P.M. Gresho, R.L. Lee, Don't suppress wiggles – they're telling you something, Computers and Fluids 9 (1981) 223–253.
[14] X. Wu, P.A. Durbin, Evidence of longitudinal vortices evolved from distorted wakes in a turbine passage, Journal of Fluid Mechanics 446 (2001) 199–228.
[15] V. Armenio, U. Piomelli, A Lagrangian mixed subgrid-scale model in generalized coordinates, Flow, Turbulence and Combustion 65 (2000) 51–81.
[16] C.A.J. Fletcher, Computational Techniques for Fluid Dynamics: Fundamentals and General Techniques, second ed., vol. 1, Springer, Berlin, 1991.
[17] P. Moin, Fundamentals of Engineering Numerical Analysis, Cambridge University Press, Cambridge, 2001.
[18] O.V. Vasilyev, High order finite difference schemes on non-uniform meshes with good conservation properties, Journal of Computational Physics 157 (2000) 746–761.
[19] R.W.C.P. Verstappen, A.E.P. Veldman, Spectro-consistent discretization of Navier–Stokes: a challege to RANS and LES, Journal of Engineering Mathematics 34 (1998) 163–179.
[20] R.W.C.P. Verstappen, A.E.P. Veldman, Direct numerical simulation of turbulence at lower costs, Journal of Engineering Mathematics 32 (1997) 143–159.
[21] A.E.P. Veldman, K. Rinzema, Playing with nonuniform grids, Journal of Engineering Mathematics 26 (1992) 119–130.